Nano Energy 39 (2017) 506–512

Contents lists available at ScienceDirect

Nano Energy

journal homepage: www.elsevier.com/locate/nanoen

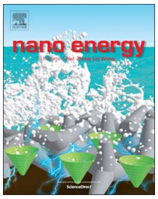

Full paper

Cu_4SnP_{10} as a promising anode material for sodium ion batteries

Danni Lan, Wenhui Wang, Quan Li*

Department of Physics, The Chinese University of Hong Kong, Shatin, New Territory, Hong Kong, China

ARTICLE INFO

Keywords:
Copper tin phosphide
Anode
Solution-liquid-solid
Sodium ion batteries

ABSTRACT

High theoretical capacity of metal phosphides makes them promising candidates for anode application in sodium ion batteries. In this work, we report a ternary compound phosphide—copper tin phosphide (Cu_4SnP_{10}) nanowires for sodium ion battery anode applications. The introduction of Cu helps to stabilize a rather high P content in the compound (as compared to Sn_4P_3, for example), enabling a high capacity of 811 mA h g^{-1} at a current density of 25 mA g^{-1} for phase pure Cn_4SnP_{10} nanowire anode. Cu incorporation is also found to effectively alleviate Sn aggregation in the anode during charge/discharge cycles, which is known as a major contributor to the faded cycle performance of Sn-P compound. On the other hand, we show that possible volume expansion and instability of the solid electrolyte interface in the Cn_4SnP_{10} nanowire anode remain as problems causing cycle instability of the electrode. By forming composite with multiwall carbon nanotubes, we demonstrate significantly improved cycle performance of the composite anode, which delivers a stable capacity of 512 mA h g^{-1} after 100th cycle at a current density of 100 mA g^{-1}. At higher current density of 1 A g^{-1}, the capacity of the composite electrode retains at 412 mA h g^{-1}, showing its good rate performance.

1. Introduction

Similarities in the physico-chemical properties between sodium ions and lithium ions and a more available sodium resource on earth make sodium ion batteries (SIBs) an attractive alternative for Li ion batteries (LIBs), especially in the application of large energy storage [1–3]. Nevertheless, unlike LIBs, the anode development in SIBs is more challenging, as graphite no longer serves a valid anode for SIBs due to the larger ion radius of Na than that of Li [4].

Among possible anode materials for SIBs, phosphorus (P) attracts much attention due to its highest theoretical capacity (2596 mA h g^{-1}) [5–7]. However, its intrinsic low conductivity (1×10^{-14} S cm^{-1}), large volume expansion (~ 390%) and unstable Na_3P formation during sodiation limit the reversible capacity and cycle stability of P electrode [8,9].

A few methods have been proposed to improve the cycling performance of P. Introducing carbon based materials to form a composite with the phosphorus, for example, red P/carbon nanotubes [10], amorphous P/carbon composites [11], P/N-doped carbon [12], and amorphous P/ordered mesoporous carbon [13], etc. are found to improve the cycle performance of the electrode, as the incorporated carbon materials are suggested to act as an interconnecting and surface-reinforcing matrix that providing conducting network and holding against the large volume change during cycling. However, these P/C composites still either suffer from rather low cyclability [10–12], or significantly reduced total capacity as one has to largely reduces the P content in the P/C composites [10,13]. When vaporization-condensation process is employed for such purpose, the distribution of red P in the pores of carbon is difficult to control [14], while flammable white P is likely to be generated during condensation process, and its removal would involve toxic CS_2 [8,13].

Forming compound with metal (metallic phosphide) serves as alternative way to stabilize the P, and at the same time, improve the electrical conductivity of the electrode (compared to pure P). A number of metal phosphides have been attempted, such as CoP [15], CuP_2 [16], Ni_2P [17], and Sn_4P_3 [18–21], etc. Relatively stable capacity of ~ 200–800 mA h g^{-1} for a few tens to 100 cycles have been reported for these metal phosphides. Among various metal phosphide, tin phosphide (Sn_4P_3) stands out as one of the promising candidate for SIBs anode [22–24]. A higher capacity (~ 400–800 mA h g^{-1}) than other transition metal phosphides has been reported. Nevertheless, the P content in Sn_4P_3 is rather low (43 at%), reducing its contribution to the overall electrode capacity (the capacity of Sn is lower that of P). In addition, the cycling performance of Sn_4P_3 remains unsatisfactory, which is generally ascribed to the volume expansion, Sn agglomeration, and the unstable interfaces with the electrolyte, with detailed mechanisms remaining unclear [25].

In the present work, we show that by introducing a third element (Cu) during the Sn-P compound growth, a trinary compound of Cu_4SnP_{10} can be formed, stabilizing a higher P content (67 at%) in

---

* Corresponding author.
E-mail address: liquan@phy.cuhk.edu.hk (Q. Li).

http://dx.doi.org/10.1016/j.nanoen.2017.07.026
Received 21 June 2017; Received in revised form 15 July 2017; Accepted 16 July 2017

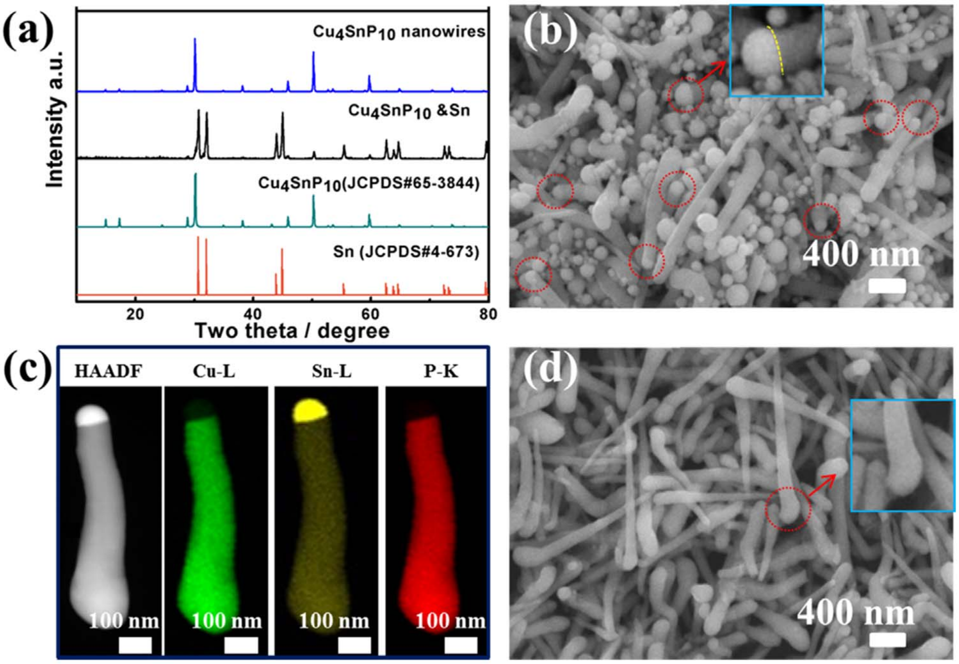

Fig. 1. (a) XRD of the Cu_4SnP_{10} & Sn sample from one pot synthesis and the pure Cu_4SnP_{10} nanowires after Sn removal; (b) SEM of the Cu_4SnP_{10} & Sn sample. Inserted image representing the enlarged selected part, in which interface between light and dark contrast is obvious; (c) STEM-EDX mapping of a single nanowire taken from samples shown in (b); (d) SEM of the pure Cu_4SnP_{10} nanowires. Inserted image representing the enlarged selected part, in which interface between light and dark contrast is absent.

the material (than in Sn_4P_3). The phosphide of this composition has a higher theoretical capacity of 1316 mA h g^{-1} (estimated based on: 4 Cu_4SnP_{10} + 135 Na^+ + 135 e^- ⇔ 40 Na_3P + $Na_{15}Sn_4$ + 16 Cu) than that of Sn_4P_3 (theoretical capacity estimated at 1133 mA h g^{-1} based on: Sn_4P_3 + 24 Na^+ + 24 e^- ⇔ 3Na_3P + $Na_{15}Sn_4$). The Cu introduction is also found to prevent the Sn agglomeration in the compound upon repeated cycles, while Sn agglomeration in Sn_4P_3 is a major factor contributing to its cycle performance decay. By effectively wrapping the Cu_4SnP_{10} nanoparticle surfaces with multi-walled carbon nanotubes (MWCNTs), we further fabricate Cu_4SnP_{10}/MWCNTs composites electrode, which shows a reversible capacity of 512 mA h g^{-1} after 100th cycle at a current density of 100 mA g^{-1}. A capacity of 412 mA h g^{-1} is obtained at a high current density of 1 A g^{-1}. The good rate capability and cycle stability make Cu_4SnP_{10}/ MWCNTs a promising candidate for sodium ion battery anode.

2. Experimental

2.1. Materials preparation and characterization

2.1.1. Synthesis of the Cu_4SnP_{10} nanowires

The synthetic procedures were similar to that of Sn_4P_3, as reported elsewhere [25]. Briefly, all the reactions were carried out in an atmosphere of high purity nitrogen, 4.5 mmol tin(II) acetylacetonate, 1 mmol copper (II) acetylacetonate and 40 mL trioctylphosphine were mixed and degassed at 120 C° for 0.5 h using a heating mantle in a flask under stirring with a reflux condenser. The mixtures were then aged at 350 C° for 2 h. After that, cooling down to room temperature, the samples were then washed and centrifuged with hexane for several times. To move the impurity of Sn and Sn-P compound, the as-prepared samples were then purified with 6 mol L^{-1} hydrochloric acid (HCl). After a second washing and centrifuging with ethanol and deionized water, pure Cu_4SnP_{10} nanowires can be obtained. The wet Cu_4SnP_{10} nanowires samples were finally dried in vacuum to black powers.

2.1.2. Synthesis of the Cu_4SnP_{10}/MWCNTs composites

Cu_4SnP_{10}/MWCNTs composites were prepared by ball milling under an argon atmosphere. The active materials (Cu_4SnP_{10} nanowires): carbon nanotubes weight ratio was set to 8:2. The weight ratio of milling balls (tungsten carbide) to powders was 40:1. The rotation speed of the mill was set to 400 rpm for 10 h.

2.2. Characterization

Scanning electron microscope (SEM, JSM-7800F, JEOL) was used to characterize the morphology and composition of the samples. Transmission electron microscopy (TEM) images were acquired on a Tecnai F20 ST (FEI) microscope operating at 200 kV. Raman analysis was performed using a Micro Raman spectrometer (RM-1000, Renishaw Co., Ltd.) with a 10 mW helium neon laser at 514 nm. The crystallinity and phases of the samples were examined by X-ray diffraction (XRD, SmartLab, Rigaku) with a Cu-Ka radiation source (d = 0.1541 nm). The electrodes that were cycled at a current density of 100 mA g^{-1} for ex-situ XRD were disassembled in an inert-gas filled glovebox, and the samples were sealed with polyimide tape (Kapton, 2 mil thickness) before being transferred to the X-ray diffractometer.

2.3. Assembly of a 2032 coin-type half-cell with Na as the anode

The electrodes were prepared by spreading a slurry of 70 wt% active materials, 20 wt% multi-walled carbon nanotubes (MWCNTs) and 10 wt% sodium carboxymethylcellulose (CMC) binder (without any other additional additive) on a copper foil substrate to form a thin film. The mass loading of the active materials within the film was about ~ 1 mg cm^{-2}. A mixture of 1 M $NaPF_6$ in propylene carbonate/ Fuoroethylene carbonate (PC/FEC, 95:5 in volume) was used as the electrolyte. Cyclic voltammetry (CV) and electrochemical impedance spectroscopy (EIS) measurements were performed on a CHI660c electrochemical workstation (ChenHua instrument Co., China). The galvanostatic charge/discharge test was conducted on a LAND CT2001A battery test system.

3. Results and discussions

The growth of the phase pure Cu_4SnP_{10} nanowires is guided by the solution-liquid-solid mechanism (SLS), which is similar to that of Sn_4P_3 nanotops growth [25]. The as-synthesized products are a mixture of Cu_4SnP_{10} and Sn as suggested by X-ray diffraction (XRD) (Fig. 1a). Scanning electron microscopy (SEM) image (Fig. 1b) shows that the product consists of nanowires and nanoparticles. Light/dark contrast can be observed in most nanowires (marked by the red circles, the yellow line in the insert shows the light/dark interface). Taking one of such nanowires for energy-dispersive X-ray (EDX) elemental mapping (Fig. 1c), an obvious Sn semi-sphere is observed at one end of the Cu_4SnP_{10} wire, and the other end of the nanowire appears to be thicker. Such morphological characteristics are consistent with the SLS growth mechanism [25]. One should note that the SLS mechanism relies on the presence of a catalyst, which is Sn in the present case, supersaturation of the product phase leads to its precipitation and growth from the catalyst particle. When the catalyst particle does not participate in the product phase formation process, the product usually grows into a wire-like morphology (trying to minimize the interfacial energy between the catalyst and newly grown phase). Otherwise the morphology of the products depends on how fast the catalyst (Sn) will be consumed during the product phase formation. In the case of Sn_4P_3, a fast consumption of Sn occurs and a morphology (nanotop) with small aspect ratio is resulted [25]. In the case of Cu_4SnP_{10}, the consumption of Sn is much slower (due to the lower ratio of Sn in Cu_4SnP_{10}), so that a wire like morphology is obtained. By removing the Sn with hydrochloric acid (HCl), phase pure Cu_4SnP_{10} nanowires (Fig. 1a, blue line) with a diameter of~ 200 nm and a length of ~ 1 µm are obtained (Fig. 1d). It is worth noting that while most phosphide materials suffer from chemical instability in air and/or acidic environment [26], Cu_4SnP_{10} is stable in both air and strong acids (hydrochloric acid, sulfuric acid, hydrofluoric acid) [27]. This unique property makes it convenient for further processing the Cu_4SnP_{10} as electrode materials for SIBs.

The phase pure Cu_4SnP_{10} nanowires are firstly assembled as the electrode for half-cell SIBs. Fig. 2a depicts the cyclic voltammetry (CV) curves of the Cu_4SnP_{10} nanowires. During the first cathodic scan, a broad peak at ~ 1 V can be ascribed to the formation of solid electrolyte interphase (SEI), another sharp peak close to the 0.01 V is mainly attributed to the initial conversion process of the Cu_4SnP_{10} to the Na_xSn_y and Na_xP_y composites. In the next cycles, two pair of peaks can be found. In comparison with the CV features of elemental Sn and P [28,29], peaks at ~ 0.45 (in the cathodic scan) and 0.9 V (in the anodic scan) can be respectively assigned to alloying and de-alloying reactions of P with Na, along with the initial alloy/de-alloy process of Na-Sn. The other pair of peaks at ~ 0.3 (in the cathodic scan)/0.7 V (in the anodic scan) relate to the further alloying, and de-alloying process of Na-Sn, respectively. Although alloying reactions (formation of Na-Sn and Na-P) start to take place at 0.45 V and 0.3 V (in the cathodic scan) after the second scan, continuous conversion persists until close to 0.01 V due to the slow activation of the anode material, which is also responsible for the capacity increase of the sample as observed in the CV of next few cycles. Similar phenomenon of the continuous increase of the capacities has been reported in Cu-Sn anodes [30], indicating the introduction of Cu may lead to higher barrier for the sodiation/desodiation reactions of the electrode materials. Capacity-voltage profile taken at a current density of 25 mA g^{-1} reveals a high discharging capacity of 1250.1 mA h g^{-1} and charging capacity of 787.8 mA h g^{-1} in the first cycle (Fig. 2b). The irreversible capacity can be assigned to the formation of SEI. In the next few cycles, capacities are relatively stabilized above 700 mA h g^{-1} with an average reaction potential in the range of 0.4–0.8 V, being consist with those in the CV data. Fig. 2c shows the cycle performance of the Cu_4SnP_{10} nanowires electrodes, a high charge capacity above 600 mA h g^{-1} can be obtained for the first 20th cycles, but fast decay occurs in the following cycles. The rate capacity is evaluated (Fig. 2d) within the first 20 cycles (excluding the effect of cycle stability). The Cu_4SnP_{10} nanowires electrodes shows reversible capacities of 811, 757, 735, 664, 543 mA h g^{-1} at current densities of 25, 100, 200, 500 and 1000 mA g^{-1}, showing good rate performance.

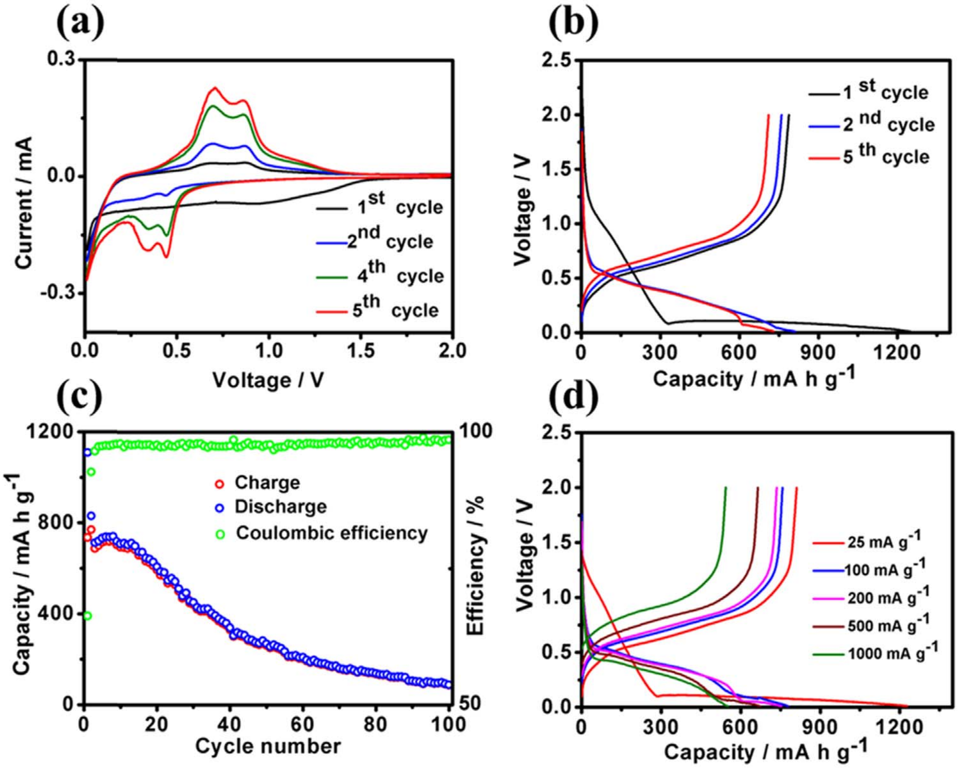

Fig. 2. Electrochemical performances of the Cu_4SnP_{10} nanowires, (a) CV curves scanned at a rate of 0.05 mV s^{-1}; (b) Charge/discharge curves obtained at a constant current density of 25 mA g^{-1}; (c) Cyclic performance measured at a current density of 100 mA g^{-1}; (d) Charge/discharge Capacities of the nanowire electrode measured at current densities of 25, 100, 200, 500 and 1000 mA g^{-1}. The electrodes were activated at a current rate of 25 mA g^{-1} for two cycles (included in (c)) before measuring at 100 mA g^{-1}.

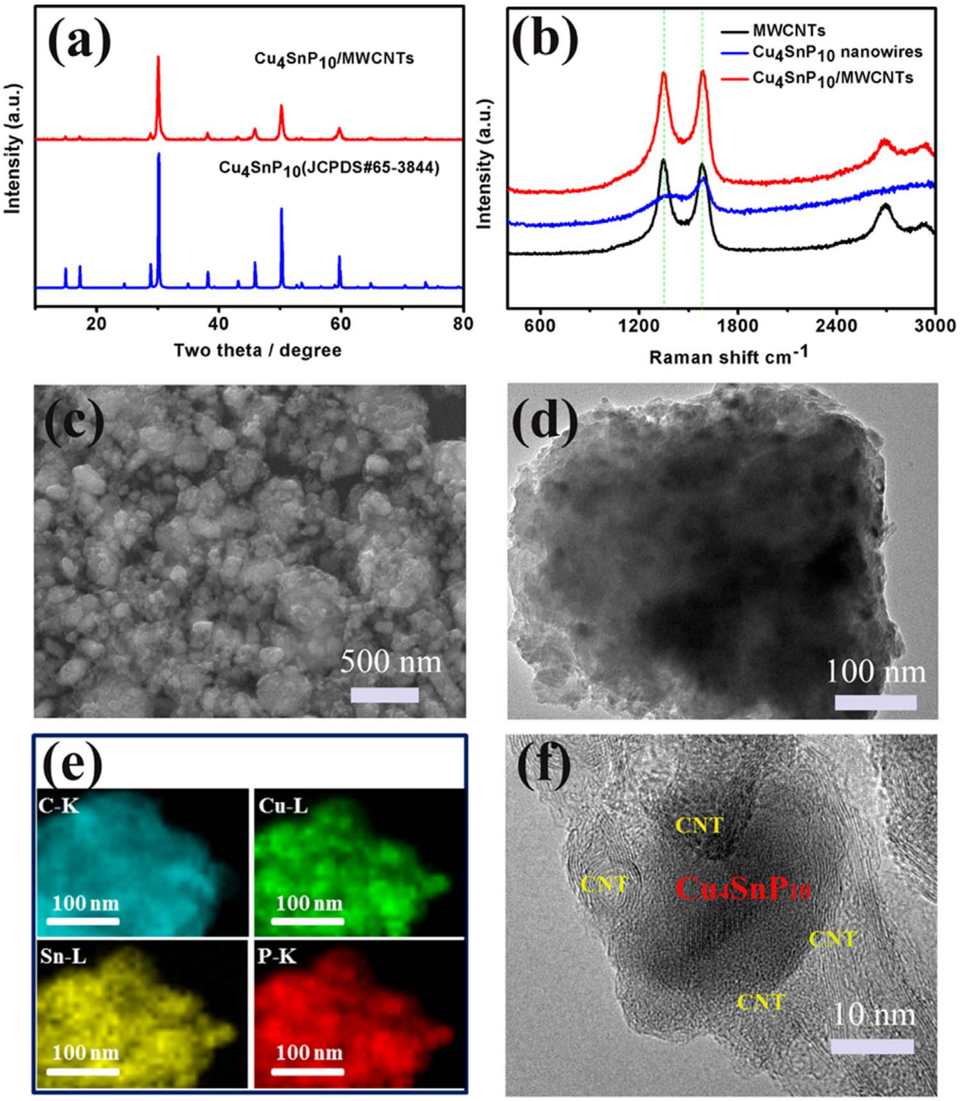

Fig. 3. (a) XRD, (b) Raman, (c) SEM, (d) Low magnification TEM, (e) STEM-EDX maps, (f) High resolution TEM of the Cu_4SnP_{10}/MWCNTs composite sample.

SEM and EDX mapping are used to investigate the morphological change of the Cu_4SnP_{10} nanowires upon repeated cycles. Fig. S1 reveals the structure of the pure Cu_4SnP_{10} nanowires after different cycles. After the first cycle, the morphology of the Cu_4SnP_{10} nanowires is preserved (Fig. S1c). After 100th cycles, although one still can discern the pseudo-one-dimensional morphology of the wires, their surfaces become rough with reduced nanowire diameter (Fig. S1e). These changes are likely resulted from the volume expansion (which is inevitable in most anodes with alloying/de-alloying as the energy storage mechanism) that pulverize the nanowires, as well as the decomposition /re-composition of unstable SEI during cycling, both factors contributing to decreased cycle stability at longer cycles. Fig. S2 presents the elemental mapping of the nanowires after 100th cycle, further confirming the damaged nanowire structure.

On the other hand, the elemental mapping of Cu_4SnP_{10} nanowires also reveals the rather uniform distribution of Sn in the sample, being always coinciding with the presence of Cu and P (Fig. S2). It is worth noting that Sn agglomeration is quite significant in the cycled sample of Sn_4P_3, serving as a major contributor to deteriorating the electrode performance upon cycling (Fig. S3a). Then the observation of uniform Sn distribution suggests that the alleviated agglomeration of Sn in the Cu_4SnP_{10} compound. This result is further confirmed by ex-situ XRD taken from the Cu_4SnP_{10} electrode after 100th cycles. In Fig. S3b, no obvious Sn peak can be identified, suggesting the Sn agglomeration should not be the reason for the faded performance of the Cu_4SnP_{10} electrode upon cycling, and one shall tackle the volume expansion and/or unstable solid electrolyte interface during cycling in order to further improve the cyclability of the electrode.

Carbonaceous materials had been successfully applied to buffer the volume expansion and enhance the stability of many alloy type of anode materials [31–33]. We then fabricate the Cu_4SnP_{10}/MWCNTs composite by ball milling, which process does not change the phase composition of Cu_4SnP_{10}. Fig. 3a shows the XRD of a representative ball milled sample. All diffraction peaks can be indexed to that of cubic Cu_4SnP_{10} (JCPDS#65–3844), and no other peak is observed. The broadened diffraction peaks suggest a smaller size of the Cu_4SnP_{10} in the Cu_4SnP_{10}/MWCNTs composite than the original nanowires (Fig. S4). Fig. 3b compares the Raman spectra of the MWCNTs, Cu_4SnP_{10} nanowire and the Cu_4SnP_{10}/MWCNTs composite samples. For pure MWCNTs, two broad bands at ~ 1350 cm^{-1} and ~ 1577 cm^{-1} and the broad and asymmetric peaks at ~ 2700–2900 cm^{-1} can be observed, corresponding to the D band (disordered; sp^3-type, i.e. C–C sigma bonding), G band (graphite or graphene characteristic; sp^2-type; i.e. unsaturated C=C entities) and 2 D band (arises from the second order of zone-boundary phonons) [34,35]. On the other hand, the Raman spectrum of Cu_4SnP_{10} only shows two weak peaks at ~ 1300–1600 cm^{-1}, which could be related to the organic carbon impurity during synthesis of the pure Cu_4SnP_{10} nanowire. After ball milling the

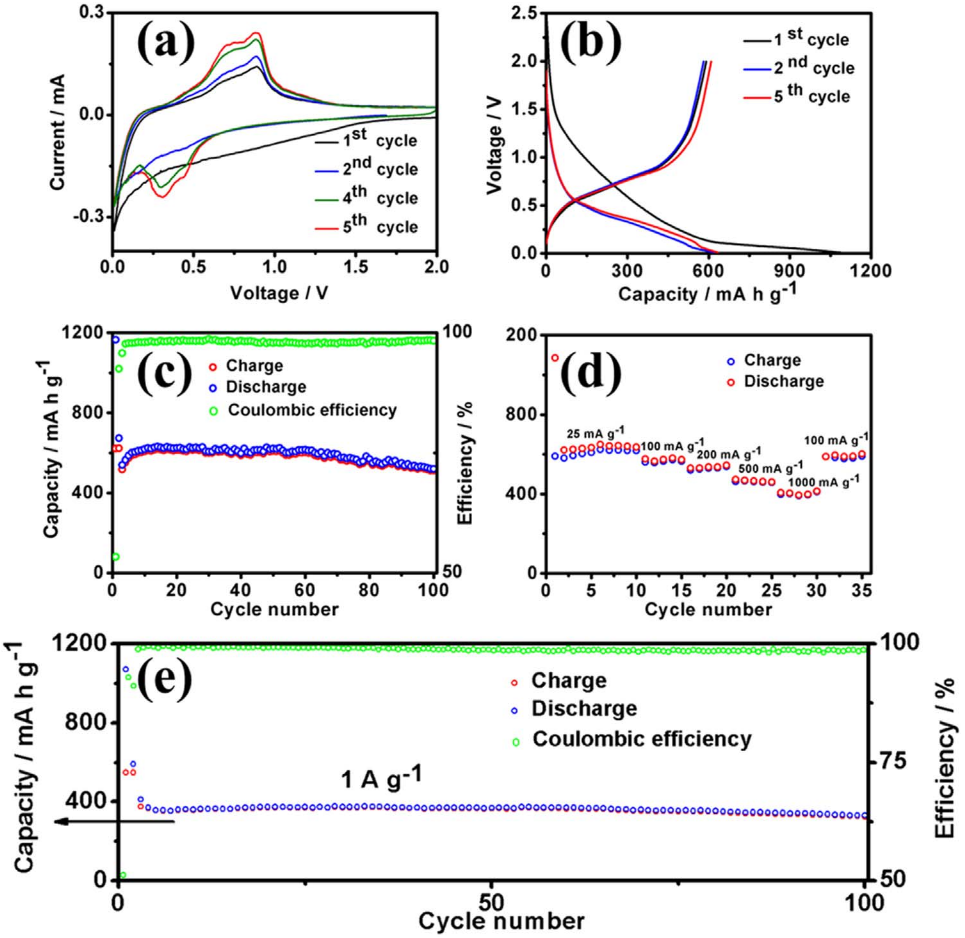

Fig. 4. Electrochemical performances of the Cu_4SnP_{10}/MWCNTs, (a) CV curves scanned at a rate of 0.05 mV s^{-1}; (b) Charge/discharge curves at a constant current density of 25 mA g^{-1}; (c) Cycle performance measured at a current density of 100 mA g^{-1}. (d) Rate performance measured at current densities of 25, 100, 200, 500 and 1000 mA g^{-1}; (e) long cycling performances of Cu_4SnP_{10}/MWCNTs at 1 A g^{-1}. All the capacities were normalized to the mass of Cu_4SnP_{10} and the electrodes for cycle performance were activated at a current rate of 25 mA g^{-1} for initial two cycles (included in (c) and (e)) before measuring at 100 mA g^{-1} or 1 A g^{-1}.

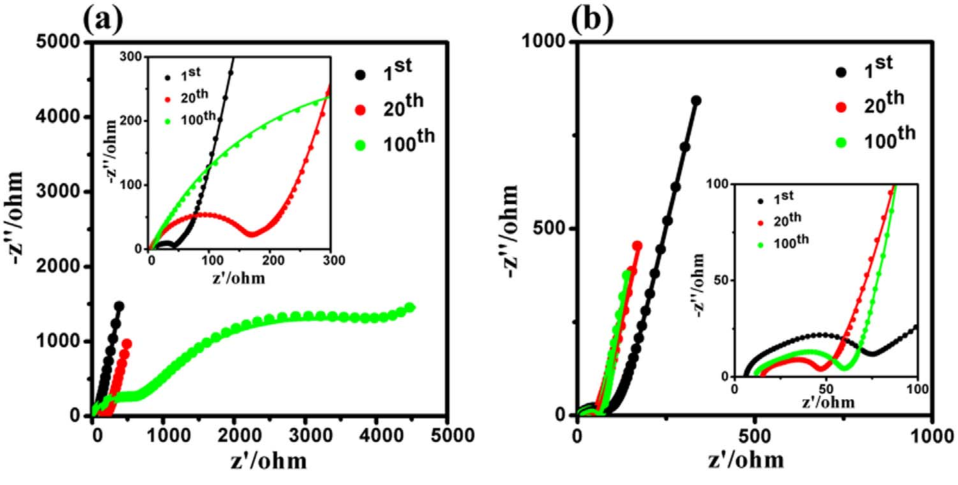

Fig. 5. Nyquist plots of the (a) pure Cu_4SnP_{10} nanowires and (b) Cu_4SnP_{10}/MWCNTs electrodes at the fully charged state during cycling. Solid symbols represent the experimental data, and lines are the fitted data based on the model of equivalent circuit shown in the Table S1.

Cu_4SnP_{10} nanowire with MWCNTs, the Raman features of the composite is similar to that of the pure MWCNTs, no obvious peaks shift or the typical P–C bond centered at ~ 700 cm^{-1} [8] can be found, indicating the nature of physical combination with little chemical change for the ball milled samples. The morphology of the Cu_4SnP_{10}/MWCNTs composites are revealed by SEM. In Fig. 3c, clusters (of hundreds nm to micron size) consisting of nanoparticles (size ~ 100 nm) can be observed, which morphology is completely different from that of the as-synthesized Cu4Sn_4P_{10} nanowires. Low magnification transmission electron microscopy (TEM) image in Fig. 3d further shows the morphology of the Cu_4SnP_{10}/MWCNTs as clusters. Fig. 3e shows the elemental maps of Cu, Sn, P, and C, taken from one of the representative clusters, disclosing the high correlation among the spatial distribution of Cn, Sn, and P; as well as the uniform distribution of carbon over the whole cluster. The high resolution TEM image taken from part of such a cluster reveals that individual Cu_4SnP_{10} nanoparticles are well wrapped by MWCNTs (Fig. 3f).

Electrochemical performance of the Cu_4SnP_{10}/MWCNTs composite is given in Fig. 4. Fig. 4a shows the CV curves of the Cu_4SnP_{10}/MWCNTs composite. During the first two cathodic scan, there is no obvious peak, mainly due to a slower diffusion kinetic originating from the larger size of the clusters and the introduction of carbon, extending the voltage for the occurrence of sodiation to a slightly broader range. In the next cycles, redox peaks at similar voltages (at 0.3–0.9 V) to that of the Cu_4SnP_{10} nanowires can be found, indicating a similar sodiation/desodiation chemistry of the Cu_4SnP_{10}/MWCNTs composite to that of the phase pure Cu_4SnP_{10} nanowires. In Fig. 4b, capacity-voltage profile shows a high discharging capacity of 1086 mA h g^{-1} and charging capacity of 591 mA h g^{-1} in the first cycle. In the next few cycles, capacities are stabilized at ~ 600 mA h g^{-1}. The lower capacity of the Cu_4SnP_{10}/MWCNTs composites than that of the pure Cu_4SnP_{10} nanowires could be caused by the larger size of the clusters, making some of the active material unassessed. The Cu_4SnP_{10}/MWCNTs composite shows a relatively stable cycling performance after the first two active cycles (Fig. 4c), a charge capacity remained at a high value of 512 mA h g^{-1}at the current density of 100 mA g^{-1} after 100th cycles. Fig. 4d plots the capacity of the Cu_4SnP_{10}/ MWCNTs composite at different current densities. Excellent rate performance of the composite electrode is observed—it delivers capacities of 621, 572, 539, 466, 412 mA h g^{-1} at the current densities of 25, 100, 200, 500 and 1000 mA g^{-1}. A slightly improved capacity (590 mA h g^{-1}) is obtained when the current density returns to 100 mA g^{-1}, likely due to the activation of the electrode in the previous charge/discharge cycles. The cycle performance of the electrode is largely enhanced as compared to that of the pure Cu_4SnP_{10} nanowires. Even being cycled at a high current density of 1 A g^{-1}, the Cu_4SnP_{10}/ MWCNTs composite delivers a stable capacity around 325 mA h g^{-1} after 100 cycles (Fig. 4e), corresponding to~80% retention of the capacity at this current density.

Electrochemical impedance spectroscopy (EIS) is used to investigate the improved stability of the Cu_4SnP_{10}/ MWCNTs composite anodes. Fig. 5 presents the EIS results of the anodes at different cycle states. The data are fitted by using an equivalent circuit and the resultant fitting parameters are listed in Table S1. For the first cycle, the diameters of the semicircle at high-medium frequency for both electrodes are of the same order. The respective surface/charge transfer resistance ($R_{sf/ct}$) values are estimated as 34.64 Ω, and 64.72 Ω for the pure Cu_4SnP_{10} nanowires and Cu_4SnP_{10}/ MWCNTs composite anodes, respectively, indicating that the initial conductivity of the pure Cu_4SnP_{10} (~ 10^{-6} S cm^{-1}) [27] is not a crucial factor for the fading of cycle performance. However, upon cycling, the R_{sf} of the pure Cu_4SnP_{10} nanowires continuously increases and at 100th cycle, it becomes 1–2 order of magnitude higher than that of the Cu_4SnP_{10}/MWCNTs composite anodes. It is also found that the cluster morphology of the Cu_4SnP_{10}/MWCNTs remain largely unchanged upon long cycles. (SEM images in the Fig. S1(b), (d), (f), and EDX mapping in Fig. S5).

A few factors contribute to the good electrochemical performance of the Cu_4SnP_{10}/MWCNTs composite electrode. The presence of Cu not only prevents Sn agglomeration during cycling, but also help to stabilize a rather high content of the P in the Cu_4SnP_{10} (as compared to Sn_4P_3), which makes a contribution to the high capacity of the electrode. The reduced size of Cu_4SnP_{10} after ball milling and the presence of interconnecting MWCNT network helps to alleviate the volume expansion of the electrode. Furthermore, the effective surface protection of the Cu_4SnP_{10} by MWCNT also contribute to the improved cycle stability of the electrode. On the other hand, many of the reported phosphide materials show very low specific capacity (< ~ 500 mA h g^{-1}, e.g. CuP_2 compounds [16]) in practice, although their theoretical capacity is high. The practical capacity of the phosphide depends on many factors, especially the kinetic ones. It's possible that higher reaction and/or diffusion barriers during sodiation/desodiation of some phosphide materials would lead to the apparently low capacity in practice. In the present work, the reversible capacity can be higher than 800 mA h g^{-1}, suggesting that the interplay among Cu, Sn and P result in reasonable reaction kinetics during sodiation/desodiation.

4. Conclusion

In conclusion, we have developed ternary compound Cu_4SnP_{10} nanoparticles for anode applications in sodium ion batteries. The high content of P in Cu_4SnP_{10} enables a higher capacity to be delivered, as compared to the most promising phosphide candidate-Sn_4P_3. The introduction of Cu in the compound is found to prevent Sn agglomeration in the electrode upon cycling—a problem identified as a major contributor to the decayed cycle performance of Sn_4P_3 electrode. By fabricating the Cu_4SnP_{10}/MWCNTs composite electrode, a high reversible capacity of 512 mA h g^{-1} at the current of 100 mA g^{-1} has been achieved after 100 cycles. At higher current density of 1 A g^{-1}, the capacity of the composite electrode retains at 412 mA h g^{-1}, showing its good rate performance. At the end of 100 cycles, ~80% capacity retention is obtained for electrode cycled at 1 A g^{-1}, demonstrating good cycling stability. Together with its chemical stability in the air and acid, the high capacity, and good cycle performance/rate performance of Cu_4SnP_{10}, as well as the cheap elements choice, make it promising for anode application in sodium ion batteries.

Conflict of interest

The authors declare no competing financial interest.

Acknowledgements

This work is supported by the RGC/GRF under Project no. 14316716.

Appendix A. Supplementary material

Supplementary data associated with this article can be found in the online version at doi:10.1016/j.nanoen.2017.07.026.

References

[1] N. Yabuuchi, K. Kubota, M. Dahbi, S. Komaba, Research development on sodium-ion batteries, Chem. Rev. 114 (2014) 11636–11682.
[2] W. Luo, F. Shen, C. Bommier, H. Zhu, X. Ji, L. Hu, Na-ion battery anodes: materials and electrochemistry, Acc. Chem. Res. 49 (2016) 231–240.
[3] L.P. Wang, L. Yu, X. Wang, M. Srinivasan, Z.J. Xu, Recent developments in electrode materials for sodium-ion batteries, J. Mater. Chem. A 3 (2015) 9353–9378.
[4] S.-W. Kim, D.-H. Seo, X. Ma, G. Ceder, K. Kang, Electrode materials for rechargeable sodium-ion batteries: potential alternatives to current lithium-ion batteries, Adv. Energy Mater. 2 (2012) 710–721.
[5] N. Yabuuchi, Y. Matsuura, T. Ishikawa, S. Kuze, J.-Y. Son, Y.-T. Cui, H. Oji, S. Komaba, Phosphorus electrodes in sodium cells: small volume expansion by sodiation and the surface-stabilization mechanism in aprotic solvent, ChemElectroChem 1 (2014) 580–589.
[6] W. Li, S. Hu, X. Luo, Z. Li, X. Sun, M. Li, F. Liu, Y. Yu, Confined amorphous red phosphorus in MOF-derived N-doped microporous carbon as a superior anode for sodium-ion battery, Adv. Mater. 29 (2017). http://dx.doi.org/10.1002/adma.201605820.
[7] W.C. Chang, K.W. Tseng, H.Y. Tuan, Solution synthesis of iodine-doped red phosphorus nanoparticles for lithium-ion battery anodes, Nano Lett. 17 (2017) 1240–1247.
[8] C. Zhang, X. Wang, Q. Liang, X. Liu, Q. Weng, J. Liu, Y. Yang, Z. Dai, K. Ding, Y. Bando, J. Tang, D. Golberg, Amorphous phosphorus/nitrogen-doped graphene paper for ultrastable sodium-ion batteries, Nano Lett. 16 (2016) 2054–2060.
[9] J. Xu, I.Y. Jeon, J. Ma, et al., Understanding of the capacity contribution of carbon in phosphorus-carbon composites for high-performance anodes in lithium ion batteries, Nano Res. 10 (2017) 1268–1281.
[10] W.J. Li, S.L. Chou, J.Z. Wang, H.K. Liu, S.X. Dou, Simply mixed commercial red phosphorus and carbon nanotube composite with exceptionally reversible sodium-ion storage, Nano Lett. 13 (2013) 5480–5484.
[11] Y. Kim, Y. Park, A. Choi, N.S. Choi, J. Kim, J. Lee, J.H. Ryu, S.M. Oh, K.T. Lee, An

amorphous red phosphorus/carbon composite as a promising anode material for sodium ion batteries, Adv. Mater. 25 (2013) 3045–3049.

[12] B. Ruan, J. Wang, D. Shi, Y. Xu, S. Chou, H. Liu, J. Wang, A phosphorus/N-doped carbon nanofiber composite as an anode material for sodium-ion batteries, J. Mater. Chem. A 3 (2015) 19011–19017.

[13] W. Li, Z. Yang, M. Li, Y. Jiang, X. Wei, X. Zhong, L. Gu, Y. Yu, Amorphous red phosphorus embedded in highly ordered mesoporous carbon with superior lithium and sodium storage capacity, Nano Lett. 16 (2016) 1546–1553.

[14] H. Gao, T. Zhou, Y. Zheng, Y. Liu, J. Chen, H. Liu, Z. Guo, Integrated carbon/red phosphorus/graphene aerogel 3D architecture via advanced vapor-redistribution for high-energy sodium-ion batteries, Adv. Energy Mater. 6 (2016). http://dx.doi.org/10.1002/aenm.201601037.

[15] W.-J. Li, Q.-R. Yang, S.-L. Chou, J.-Z. Wang, H.-K. Liu, Cobalt phosphide as a new anode material for sodium storage, J. Power Sources 294 (2015) 627–632.

[16] F. Zhao, N. Han, W. Huang, J. Li, H. Ye, F. Chen, Y. Li, Nanostructured CuP_2/C composites as high-performance anode materials for sodium ion batteries, J. Mater. Chem. A 3 (2015) 21754–21759.

[17] C. Wu, P. Kopold, P.A. van Aken, J. Maier, Y. Yu, High performance graphene/Ni_2P hybrid anodes for lithium and sodium storage through 3D yolk-shell-like nanostructural design, Adv. Mater. 29 (2017). http://dx.doi.org/10.1002/adma.201604015.

[18] J. Qian, Y. Xiong, Y. Cao, X. Ai, H. Yang, Synergistic Na-storage reactions in Sn_4P_3 as a high-capacity, cycle-stable anode of Na-ion batteries, Nano Lett. 14 (2014) 1865–1869.

[19] X. Fan, T. Gao, C. Luo, F. Wang, J. Hu, C. Wang, Superior reversible tin phosphide-carbon spheres for sodium ion battery anode, Nano Energy 38 (2017) 350–357.

[20] J. Mao, X. Fan, C. Luo, C. Wang, Building self-healing alloy architecture for stable sodium-ion battery anodes: a case study of tin anode materials, ACS Appl. Mater. Interfaces 8 (2016) 7147–7155.

[21] X. Fan, J. Mao, Y. Zhu, C. Luo, L. Suo, T. Gao, F. Han, S.-C. Liou, C. Wang, Superior stable self-healing SnP_3 anode for sodium-ion batteries, Adv. Energy Mater. 5 (2015). http://dx.doi.org/10.1002/aenm.201500174.

[22] Q. Li, Z. Li, Z. Zhang, C. Li, J. Ma, C. Wang, X. Ge, S. Dong, L. Yin, Low-temperature solution-based phosphorization reaction route to Sn_4P_3/reduced graphene oxide nanohybrids as anodes for sodium ion batteries, Adv. Energy Mater. 6 (2016). http://dx.doi.org/10.1002/aenm.201600376.

[23] J. Liu, P. Kopold, C. Wu, P.A. van Aken, J. Maier, Y. Yu, Uniform yolk–shell Sn_4P_3@C nanospheres as high-capacity and cycle-stable anode materials for sodium-ion batteries, Energy Environ. Sci. 8 (2015) 3531–3538.

[24] Y. Kim, Y. Kim, A. Choi, S. Woo, D. Mok, N.S. Choi, Y.S. Jung, J.H. Ryu, S.M. Oh, K.T. Lee, Tin phosphide as a promising anode material for Na-ion batteries, Adv. Mater. 26 (2014) 4139–4144.

[25] D. Lan, W. Wang, L. Shi, Y. Huang, L. Hu, Q. Li, Phase pure Sn_4P_3 nanotops by solution-liquid-solid growth for anode application in sodium ion batteries, J. Mater. Chem. A 5 (2017) 5791–5796.

[26] H. Pfeiffer, F. Tancret, M.-P. Bichat, L. Monconduit, F. Favier, T. Brousse, Air stable copper phosphide (Cu_3P): a possible negative electrode material for lithium batteries, Electrochem. Commun. 6 (2004) 263–267.

[27] N.A. Goryunova, V.M. Orlov, V.I. Sokolova, G.P. Shpenkov, E.V. Tsvetkova, Investigation of some properties of ternary compound single crystals in the Cu–Sn–P system, Phys. Status Solidi 3 (1970) 75–87.

[28] J. Qian, X. Wu, Y. Cao, X. Ai, H. Yang, High capacity and rate capability of amorphous phosphorus for sodium ion batteries, Angew. Chem. 52 (2013) 4633–4636.

[29] Y. Xu, Y. Zhu, Y. Liu, C. Wang, Electrochemical performance of porous carbon/tin composite anodes for sodium-ion and lithium-ion batteries, Adv. Energy Mater. 3 (2013) 128–133.

[30] Y.M. Lin, P.R. Abel, A. Gupta, J.B. Goodenough, A. Heller, C.B. Mullins, Sn-Cu nanocomposite anodes for rechargeable sodium-ion batteries, ACS Appl. Mater. Interfaces 5 (2013) 8273–8277.

[31] Z. Liu, X.-Y. Yu, X.W. Lou, U. Paik, Sb@C coaxial nanotubes as a superior long-life and high-rate anode for sodium ion batteries, Energy Environ. Sci. 9 (2016) 2314–2318.

[32] Y. Liu, N. Zhang, L. Jiao, Z. Tao, J. Chen, Ultrasmall Sn nanoparticles embedded in carbon as high-performance anode for sodium-ion batteries, Adv. Funct. Mater. 25 (2015) 214–220.

[33] Y. Zhao, X. Li, B. Yan, D. Li, S. Lawes, X. Sun, Significant impact of 2D graphene nanosheets on large volume change tin-based anodes in lithium-ion batteries: a review, J. Power Sources 274 (2015) 869–884.

[34] D. Zhou, M. Peer, Z. Yang, V.G. Pol, F.D. Key, J. Jorne, H.C. Foley, C.S. Johnson, Long cycle life microporous spherical carbon anodes for sodium-ion batteries derived from furfuryl alcohol, J. Mater. Chem. A 4 (2016) 6271–6275.

[35] H. Wang, Y. Zhang, W. Sun, H.T. Tan, J.B. Franklin, Y. Guo, H. Fan, M. Ulaganathan, X.-L. Wu, Z.-Z. Luo, S. Madhavi, Q. Yan, Conversion of uniform graphene oxide/polypyrrole composites into functionalized 3D carbon nanosheet frameworks with superior supercapacitive and sodium-ion storage properties, J. Power Sources 307 (2016) 17–24.

Danni Lan received her Bachelor degrees in physics and chemistry from the Central China Normal University in 2015. She is currently pursuing her Ph.D. degree at The Chinese University of Hong Kong. Her research now involves the synthesis of functional materials and its application for Na-ion batteries.

Wenhui Wang received his Bachelor degree in Engineering from Harbin Institute of Technology in 2013. He is currently pursuing his Ph.D. degree at The Chinese University of Hong Kong. His research interests mainly focus on electrode materials for Li/Na-ion batteries with aqueous/organic electrolyte.

Quan Li received her Ph.D. in Materials Science and Engineering from Northwestern University in 2001. She joined The Chinese University of Hong Kong as an assistant professor in 2002, and was promoted to full professor in 2011. Her research focuses on functional materials, including the fabrication and assembly of nanomaterials, characterizations and measurements of individual nanostructures, and their applications in energy and biomedicine.